RESEARCH ARTICLE

Key Points:
- SED-TOI structure developed twice during the same storm
- Northern initial phase and southern main phase scenarios provide evidence
- Over Asia, SED did not evolve into TOI due to long distance from pole

Correspondence to:
I. Horvath,
ihorvath@itee.uq.edu.au

Storm-enhanced plasma density and polar tongue of ionization development during the 15 May 2005 superstorm

Ildiko Horvath[1] and Brian C. Lovell[1]

[1]Security and Surveillance Research Group, School of Information Technology and Electrical Engineering, University of Queensland, Brisbane, Queensland, Australia

Abstract We investigate the ionosphere's global response to the 15 May 2005 superstorm in terms of storm evolution and ionospheric electrodynamics. Our aim is to study the global distribution of plasma and the resultant large-scale ionospheric features including the equatorial ionization anomaly (EIA), storm-enhanced density (SED), and polar tongue of ionization (TOI). We have combined multi-instrument ionospheric data, solar and terrestrial magnetic data, and polar convection maps. Results reveal the prompt penetration of the interplanetary electric field to the polar region and then to the equator with a dusk-to-dawn polarity during the initial phase and with a dawn-to-dusk polarity during the main phase. This drove during the initial phase a weak eastward equatorial electrojet (EEJ) in the American sector at nighttime and a weak westward EEJ in the Indian-Australian sector at daytime. During the main phase, these EEJs intensified and changed polarities. SED and polar TOI development was observed prior to and during the initial phase at evening-premidnight hours over North America and during the main phase in the south at afternoon-evening hours in the Australian sector. During the main phase and early in the recovery phase, the EIA-SED structure was well formed in the Asian longitude sector. Then, polar TOI development was absent in the north because of the long distance from the magnetic pole but was supported in the south because of the closeness of daytime cusp and magnetic pole. Thus, the EIA-SED-TOI structure developed twice but each time in a different longitude sector and with different characteristics.

1. Introduction

During geomagnetic storms, the interplanetary electric field (IEF) becomes transferred to the high-latitude ionosphere and thus strongly influences both the ionospheric electrodynamics by generating various electric (**E**) fields and the polar plasma convection [*Gonzales et al.*, 1999]. The various **E** fields generated include the prompt penetration **E** field (PPEF) [*Vasyliunas*, 1972; *Kelley et al.*, 1979], the ionospheric disturbance dynamo **E** field (DDEF) [*Blanc and Richmond*, 1980], the equatorial polarization **E** field [*Balan and Bailey*, 1995], and the subauroral polarization stream (SAPS) **E** field [*Foster and Burke*, 2002]. As these disturbance **E** fields intensify, plasma transport becomes enhanced and polar convection expands to lower latitudes carrying significant amount of high-density and solar-produced ionospheric plasma from the afternoon sector toward the noon meridian [*Foster et al.*, 2005]. Thus, the various **E** field effects together with the mechanical wind effects [*Balan et al.*, 2010, 2013] significantly redistribute and structure the ionospheric plasma.

The major stages of plasma redistribution include the uplift of low-latitude dayside ionosphere by the undershielding eastward PPEF and the following redistribution of high-density solar-produced ionospheric plasma to middle and high latitudes by the SAPS **E** field. However, this eastward PPEF can be greatly enhanced by the equatorial eastward polarization **E** field, particularly over the Atlantic due to the effects of the South Atlantic Magnetic Anomaly (SAMA) [*Foster and Erickson*, 2013]. Consequently, the equatorial ionization anomaly (EIA) becomes significantly enhanced as the underlying forward plasma fountain [*Balan and Bailey*, 1995] strengthens into a superfountain [*Tsurutani et al.*, 2004]. Furthermore, unstable conditions created by the eastward PPEF-related uplift also affect a wide latitude region around the equator. Due to the generalized Rayleigh-Taylor (R-T) instability processes [*Ott*, 1978], plasma bubbles form in the equatorial region [*Basu et al.*, 2010; *Huang et al.*, 2012] and at middle latitudes on the nightside [*Foster and Rich*, 1998; *Basu et al.*, 2001]. Moreover, the SAPS **E** field erodes the overlying outer plasmasphere in the dusk sector [*Foster and Burke*, 2002] causing the development of large SED plumes [*Foster et al.*, 2002] and thus leads

to the development of SED features on the equatorward edge of the midlatitude trough [*Foster*, 1993]. As the two-cell plasma convection turns poleward in the noon sector, the SED plume plasma enters the polar cap and forms a polar TOI [*Foster et al.*, 2005]. However, rapid antisunward polar cap convection is crucial for TOI formation. This usually occurs along the 1200–2300 magnetic local time (MLT) axes [*Moen et al.*, 2008].

Recent studies focusing on the dynamics of superstorms demonstrate that those longitude sectors, which cover the local dusk sector during the main phase, are the most severely impacted. Impacts are caused by plasma structuring via the development of plasma bubbles and by plasma redistribution resulting in the development of SED and polar TOI. *Basu et al.* [2005, 2007, 2010] studied equatorial and low-latitude plasma bubbles and related Global Positioning System (GPS) signal scintillations occurring in the main phase at local dusk. Their results demonstrate that the longitude sector of intensive scintillation activity occurring during main phase can be predicted by specifying the local dusk sector. *Foster et al.* [2005], *Foster and Vo* [2002], and *Foster* [2008] reported the repeated occurrence of SED plume over the southeastern region of the North American continent during different superstorms unfolding in the local evening/nighttime sector. Their studies conclude that the SED plume longitude-specific occurrence at ~2100–2300 UT is associated with the passage of the sunset terminator into the SAMA region, while the anomalously weak magnetic field in the Atlantic sector makes the SAPS **E** field most effective in transporting the SED plume sunward and thus forming a polar TOI. Verified by modeling studies, the geophysical conditions are naturally favorable for SED and polar TOI development in the North American sector [*Sojka et al.*, 2012]. But according to individual observations of different storm studies, SED can also develop elsewhere such as over South America [*Foster and Coster*, 2007], Europe and Asia [*Yizengaw et al.*, 2006, 2008], and Japan [*Maruyama*, 2006]. Furthermore, *Coster et al.* [2007] reported recently that SED can also occur in its best developed form during the same storm in various longitude sectors at ~1200 MLT. Since SED and SAPS events remain fixed near local noon and drift westward with an almost corotational speed, the same SED development can be observed in those different longitude sectors that cover the local noon hours [*Coster et al.*, 2007] as the geomagnetic storm unfolds. *Coster et al.* [2007] presented a set of GPS total electron content (TEC) maps covering the 2 October 2001 geomagnetic storm ($Kp = 6$) and demonstrating the SED-SAPS structure's westward drift from Asia through Europe to North America. Finally, the study of *Coster et al.* [2007] concludes from these and other observations (e.g., 1 October 2001 and 18 April 2002) that the repeatability of SED and SAPS events is due to the systematic nature of the coupled thermosphere-ionosphere-magnetosphere system.

We note that the above-described studies demonstrate also that during the various storms and at different Kp levels, the intensity of EIA, SED, and SAPS events is different. A case like this is presented in this study. Here we investigate the temporal variation of SED and SAPS events at different Kp levels during the 15 May 2005 geomagnetic superstorm. To highlight some of the major findings, our results reveal the development of SED and TOI features over North America prior to and during the initial phase ($Kp = 6-$) and in the Asian-Australian longitude sector late in the initial phase ($Kp = 6-$) and early in the main phase ($Kp = 8+$). Although the EIA-SED structure was well developed during the main phase over Asia, the feature of polar TOI in the north did not appear.

2. Database and Methodology

We have constructed a complex multi-instrument database, applied a multitechnique methodology, and utilized our tailor-made software packages for data processing in order to carry out a comprehensive study on the 15 May 2005 superstorm. Our database contains ground- and space-based data. These include Global Positioning System (GPS) total electron content (TEC; TECU (total electron content unit), where 1 TECU = 10^{16} el/m^2) data from 402 ground-based stations processed by the Jet Propulsion Laboratory (JPL) Global Ionosphere Map (GIM) program [*Orus et al.*, 2005] and space-based TOPEX TEC values that we have computed by utilizing the over-the-ocean radar data from cycle 466 of the TOPEX/Poseidon mission [*Horvath*, 2006]. We have also made use of the multi-instrument in situ measurements of the Defense Meteorological Satellite Program (DMSP) and constructed various profiles. These measurements include ion density (Ni; i$^+$/cm^3), electron temperature (T_e; K), cross-track plasma drifts (V_Y,V_Z; m/s) in the east-west horizontal or zonal (Y) and north-south or vertical (Z) directions, and cross-track plasma flows (F_Z; i$^+$/(cm^3 s))

Table 1. List of the Various Ground-Based Stations Providing Data for This Study

| Station Name | Geographic | | Geomagnetic |
	Latitude (°N)	Longitude (°E)	Latitude (°N)
Alibag (ABG)	18.64	72.87	10.19
Chichijima (CBI)	27.10	142.18	18.47
Dyess (DS932)	32.4	260.30	41.31
Fredericksburg (FRD)	38.21	282.63	48.40
Huancayo (HUA)	−12.04	284.68	−1.71
Iqaluit (IQA)	63.75	291.48	73.98
Jicamarca (JIC)	−11.92	281.03	−1.55
Millstone Hill (MHJ45)	42.60	288.5	54.40
Muntinlupa (MUT)	14.37	121.02	3.58
Piura (PIU)	−5.01	278.93	5.11
Point Arguello (PA836)	35.6	239.4	41.20
Poste De La Beli (PBQ)	55.3	282. 20	65.45
San Juan (SJG)	18.38	293.88	28.31
Thule (THL)	77.48	290.83	87.68
Trivandrum (TVM)	8.55	76.90	0.29

computed as $Ni \times V$ [*Horvath*, 2007]. Ionosonde f_oF_2 (MHz) data, taken by a few ground-based observatories (see Table 1), monitored ionospheric conditions via N_mF_2 (el/m^3) values computed as $1.24(f_oF_2)^2 \times 10^{10}$ [*Davies and Liu*, 1991]. For monitoring the underlying geomagnetic activity and geomagnetic field variation at some specified locations (see Table 1), we have employed a small collection of geomagnetic indices and ground-based magnetometer data, respectively. Geomagnetic indices include the 1 min time resolution *SYM-H*, *ASY-H*, and *AE* data (in nT) plus the 3 h *Kp* values. We have also made use of interplanetary magnetic field (IMF) and solar plasma measurements from the Advanced Composition Explorer (ACE) and Wind satellites. As the ACE satellite was positioned at ~(249.16; 8.75;−12.56)R_E in GSE coordinate system, a ~33 min extra time was added to the ACE data permitting comparison between IMF and geomagnetic signatures. In line with the Wind satellite location of ~(210.12; 88.86; −2.00)R_E, the Wind data were delayed with ~30 min and were utilized to compute the solar wind motional zonal **E** field (IEF **E**$_Y$; mV/m) as $-\mathbf{V_X} \times \mathbf{B_Z}$ [*Mannucci et al.*, 2005] where **V**$_X$ (km/s) is the solar wind velocity in the X direction and **B**$_Z$ (nT) is the IMF's Z component. By employing the 15 min polar cap north (PCN; mV/m) index from Thule (see Table 1), we have also modeled the cross-polar cap potential (PCP) drop as Φ_{PC} (kV) $= 19.35\mathrm{PCN} + 8.78$ [*Troshichev et al.*, 1996].

3. Results and Interpretations

3.1. Evolution of the 15 May 2005 Superstorm

Figure 1 (top) is constructed with Wind solar plasma and level 2 ACE interplanetary magnetic field measurements and with geomagnetic indices. These time series depict the nature of the 15 May 2005 geomagnetic superstorm that was one of the most intense storms of the declining phase of solar cycle 23 [*Bisi et al.*, 2010]. An Earth-directed coronal mass ejection (CME) erupted two solar flares at 1630 UT on 13 May 2005. Marking the time of sudden commencement (SC) at ~0240 UT, the arrival of the CME's leading edge accelerated the solar wind (from 475 to 900 km/s) and also increased the solar proton density (from 4 to 28 p$^+$/cm^3). As the forward shock hit the Earth's magnetosphere, suddenly and simultaneously, *SYM-H*, *ASY-H*, *AE*, and modeled Φ_{PC} increased. Meanwhile, the IMF **B**$_Z$ turned northward reaching 25 nT from a southward (−5 nT) polarity. This SC marked also the onset of an unusually long initial phase lasting until ~0600 UT, for more than 3 h [*Bisi et al.*, 2010]. According to the high *Kp* index (6−) during 0000–0600 UT, there was a magnetically disturbed period starting before the initial phase commenced. Then, the IMF was southward directed (**B**$_Z$ = −5 nT) implying geomagnetic reconnection, and AE increased (from 58 to 650 nT) implying energy injections. The main phase began at ~0600 UT with the sudden southward turning of **B**$_Z$ from 50 nT and with the sudden increase of modeled Φ_{PC} from 120 kV. Under southward IMF conditions, maximizing at −45 nT, there were some periodic *ASY-H* increases. As the suddenly decreasing *SYM-H* reached a minimum of −305 nT, it registered the beginning of the recovery phase at ~0820 UT. During the main phase (0600–0820 UT), *Kp* reached 8+ and 8−. A series of energy injections is indicated by the repeated increase of *AE* implying also the occurrence of a series of substorms, one during each geomagnetic storm phase. Previously investigated by *Kozyreva and Kleimenova* [2007], the initial phase-related substorm is known as "polar cap substorm" that was caused by hydromagnetic waves penetrating from the magnetosphere to the polar cap. On the storm day of 15 May, the total daily sum of *Kp* index reached 45+. Quiet day conditions are represented by the previous day, 14 May, when the *Kp* daily total sum was 12 +.
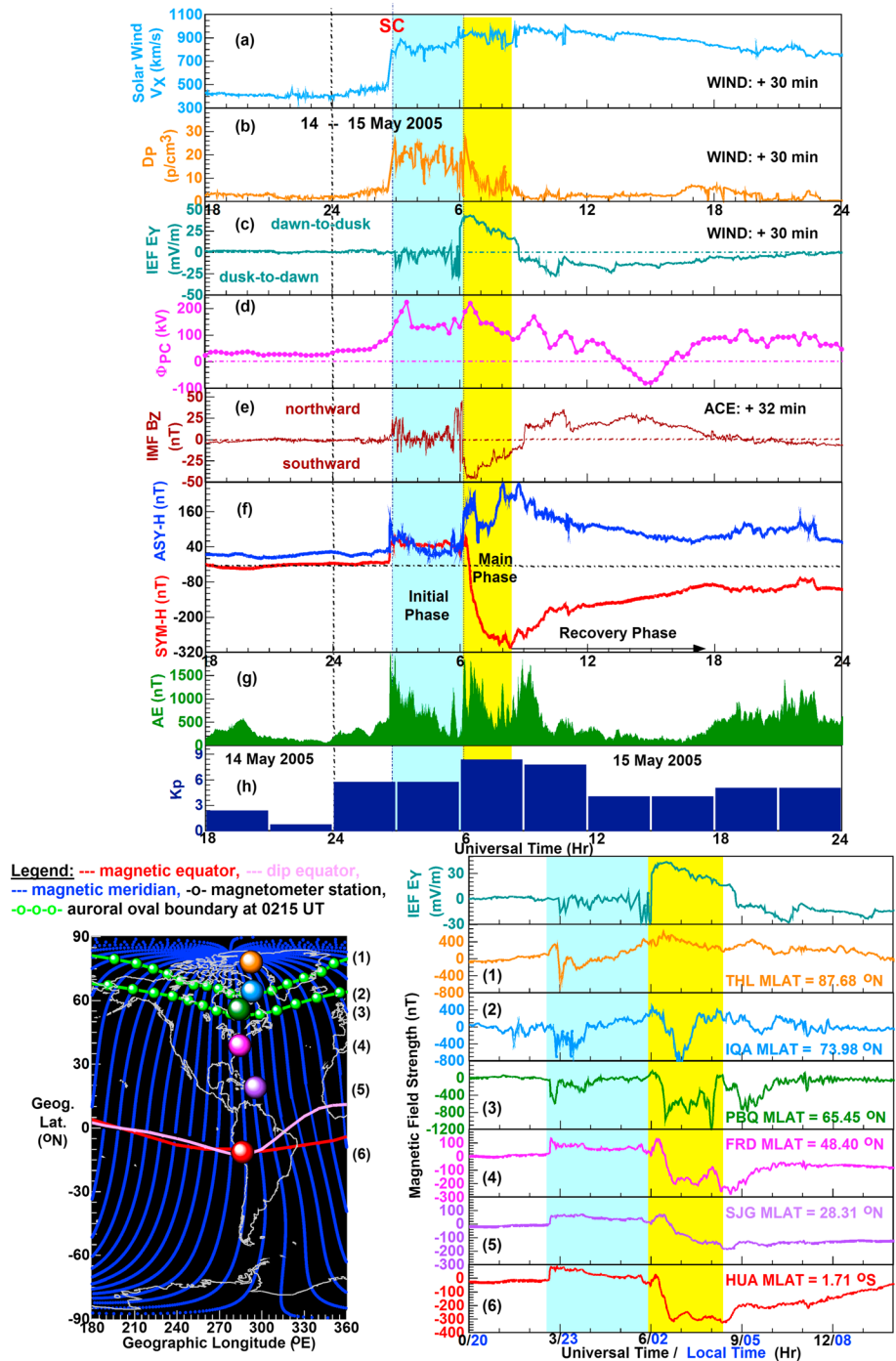
Figure 1. (top) A small collection of line plots depicts interplanetary and geomagnetic conditions and the nature of the 15 May 2005 superstorm. (bottom) The map shows the data-providing magnetometer stations' locations. The *X* component line plot series, indicating magnetic field strength, depicts stormrelated magnetic field variations in the American longitude sector.

Figure 1 (bottom) is constructed for the American sector with the time series of IEF **E**$_Y$ and *X* component geomagnetic data covering a larger time period of the initial and main phases during the local nighttime hours. Since ionospheric contribution is weak or absent at nighttime due to the low ionospheric conductivity, we could observe magnetospheric effects. As the map illustrates, the data-providing magnetometer stations cover northern latitudes from the magnetic North Pole to the magnetic dip equator at similar

magnetic meridians. We have also plotted the northern auroral oval boundaries for 0215 UT by utilizing data provided by Oval Variation, Assessment, Tracking, Intensity, and Online Nowcasting (OVATION) (http://sd-www.jhuapl.edu/Aurora/ovation/ovation_display.html). The IEF E_Y line plot illustrates some negative bays during the initial phase, and the development of a strong positive or dawn-to-dusk component during the main phase when strong magnetic reconnection allowed the injection of a large number of particles into the magnetosphere. Meanwhile, the X component line plots depict during the initial phase, some corresponding negative bays at auroral and polar cap latitudes plus some sudden positive increases at middle and low latitudes. During the main phase, the sharp decrease of geomagnetic field strength is obvious from auroral to equatorial latitudes.

According to our interpretation, these line plots illustrate some IEF E_Y-related geomagnetic perturbations seen in the X component data at low and middle latitudes where magnetospheric currents contributed mostly during the local nighttime hours (2200–0430 LT; 0200–0830 UT) as the ionospheric contribution was weak or absent. We also highlight the strong similarity between the negative bays seen during 0230–0400 UT in the IEF E_Y and X component data at auroral and polar latitudes. These similarities imply that the effects of IEF E_Y, caused by the polar cap substorm-related hydromagnetic waves [*Kozyreva and Kleimenova*, 2007], penetrated from the magnetosphere to the auroral ionosphere (see IQA line plot showing strongest signatures) and from there to the polar ionosphere. As the magnetosphere became compressed due to the forward shock at the SC, the magnetopause moved closer to Earth. Then, the sudden growth of solar wind dynamic pressure intensified the magnetospheric currents causing sharp geomagnetic field intensifications at low and middle latitudes. During the main phase, the similar IEF E_Y and polar cap X component variations suggest that an undershielding PPEF was communicated to the polar cap. Meanwhile, the suddenly decreasing solar wind dynamic pressure decreased the X component at low and middle latitudes [*Russell and Ginskey*, 1995].

3.2. Global TEC Response to Storm-Related Disturbances

We have studied the global TEC response to this superstorm in the setting of underlying electrodynamic processes. Figure 2 is constructed for the time period of 0000–1200 UT to study the driver-response relationship between the solar wind-driven disturbances and the resultant ionospheric plasma convection and plasma distribution.

Figure 2 (top) illustrates the time series of AE and PCN line plots together. Their nearly simultaneous enhancements demonstrate a strong positive correlation between them. Since the AE index is a good proxy for Joule heating [e.g., *Ahn et al.*, 1983] generated by the increased solar wind dynamic pressure [*Palmroth et al.*, 2004] and the PCN index is a representative of the polar plasma convection and convection **E** field [*Troshichev et al.*, 1996], the positive correlation of AE and PCN demonstrates a driver-response relationship between the solar wind and the electrodynamics of the polar and auroral ionospheres. A set of $\delta\Delta H$ time series—computed as $\Delta H_{(equ)} - \Delta H_{(nonequ)}$, where $\Delta H = H_{(storm\ time)} - H_{(quiet\ time)}$ [*Anderson et al.*, 2002]—is constructed for the Indian (~75°E; geographic), Australian (~150°E), and American (~300°E) longitude sectors.

According to our interpretation, these $\delta\Delta H$ plots illustrate how the strength of the equatorial electrojet (EEJ) varied due to the net disturbance **E** field since we could not separate PPEF and DDEF effects and provide also an indication of the F region net equatorial vertical **E** × **B** drift or zonal **E** field variation. Starting with the Indian sector, the $\delta\Delta H_{(TRI)-(ABG)}$ line plot depicts in the initial phase—when IEF E_Y was dusk-to-dawn-oriented—a weak westward EEJ (abbreviated as w-EEJ) that turned into a strong eastward EEJ (abbreviated as e-EEJ) by the main phase onset. During the main phase, when IEF E_Y had a dawn-to-dusk polarity, this e-EEJ gradually turned into a strong w-EEJ that started weakening early in the recovery phase. Although we utilized hourly values for the Indian sector, according to data availability in the public domain, our results are in good agreement with the more accurate results of *Dashora et al.* [2009] obtained with 1 min data. Continuing with the Australian sector and in this storm phase sequence, the $\delta\Delta H_{(MUN)-(CBI)}$ line plot tracked a weak w-EEJ, followed by a gradually intensifying e-EEJ, which maximized and then started weakening. In the American sector, the $\delta\Delta H_{(JIC)-(PIU)}$ line plot detected a weak e-EEJ, followed by a strong w-EEJ, which became very weak and turned into an e-EEJ that increased gradually.

In the bottom of Figure 2, a series of 2-hourly GPS TEC maps constructed with JPL GIM data are shown, and the local time (LT) values are indicated for the above specified longitude sectors. One of the most prominent
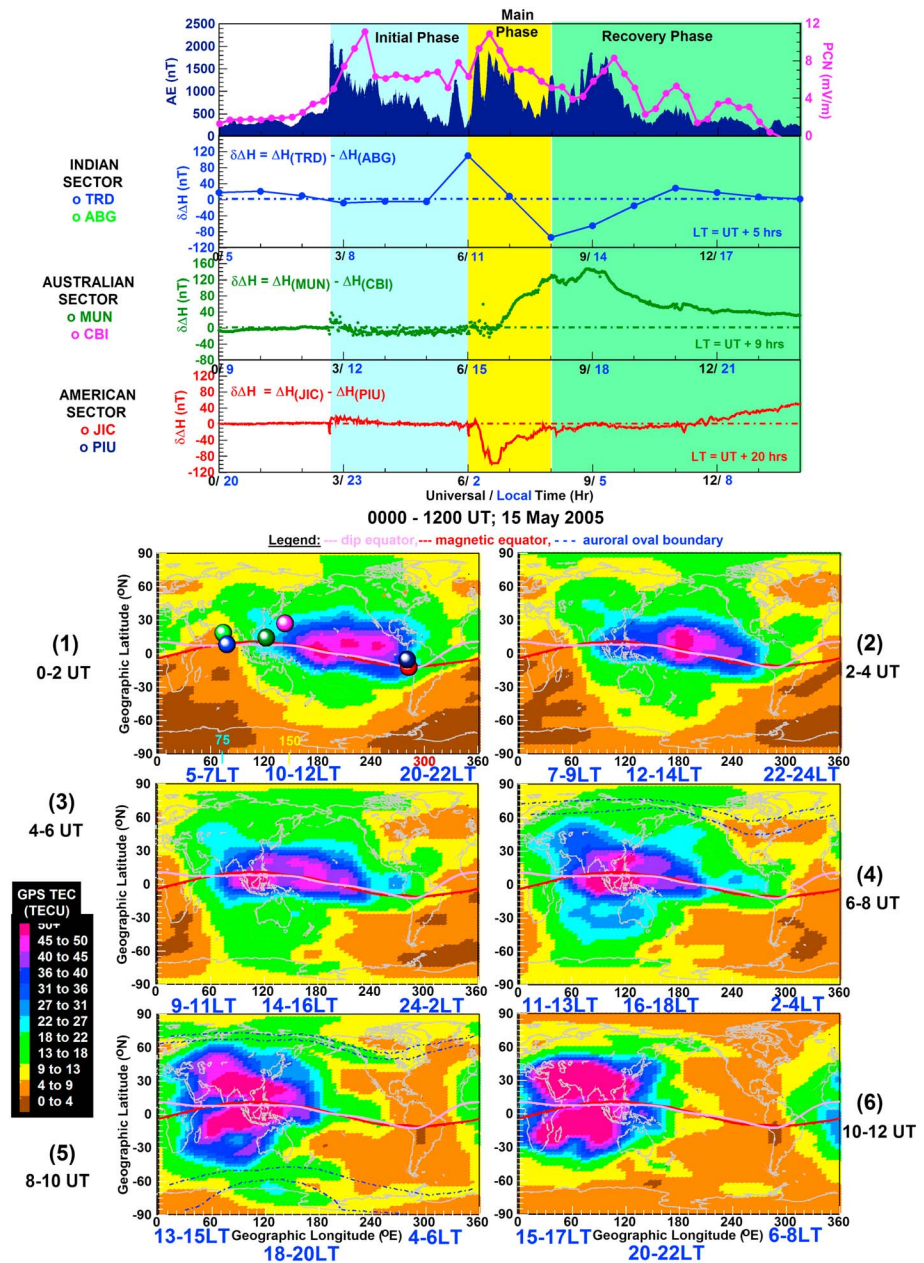
Figure 2. (top) The line plots depict the simultaneous intensifications of asymmetric ring current and cross-PCP drop, plus a series of e-EEJ and w-EEJ events occurring in the Indian, Australian, and American longitude sectors, respectively. (bottom) The GIM TEC maps demonstrate in 2 h intervals the ionosphere's global response to these geomagnetic and electrodynamic variations. The first map illustrates the locations of magnetometer stations utilized. In all maps, LT values are indicated for 75°E, 150°E, and 300°E geographic longitudes.

ionospheric features tracked is the EIA (>50 and 45–50 TECU; indicated in red and pink, respectively) that was well developed during 0000–0600 UT over the Pacific. Furthermore, the EIA appeared with a northern SED plume (36–40 TECU; indicated in dark blue) in the Asian longitude region during 0600–0800 UT in the main phase. Both at northern and at southern latitudes, the EIA-SED structure further expanded (45–50 TECU; indicated in pink) during 0800–1000 UT, early in the recovery phase. A large and enhanced TEC region (>50 TECU; indicated in red) developed over the Eastern Hemisphere during 1000–1200 UT as the recovery phase continued. Appearing as a less prominent feature, the TEC maps tracked a polar TOI (13–18 TECU; indicated in light green) during 0200–0800 UT entering the northern polar cap region
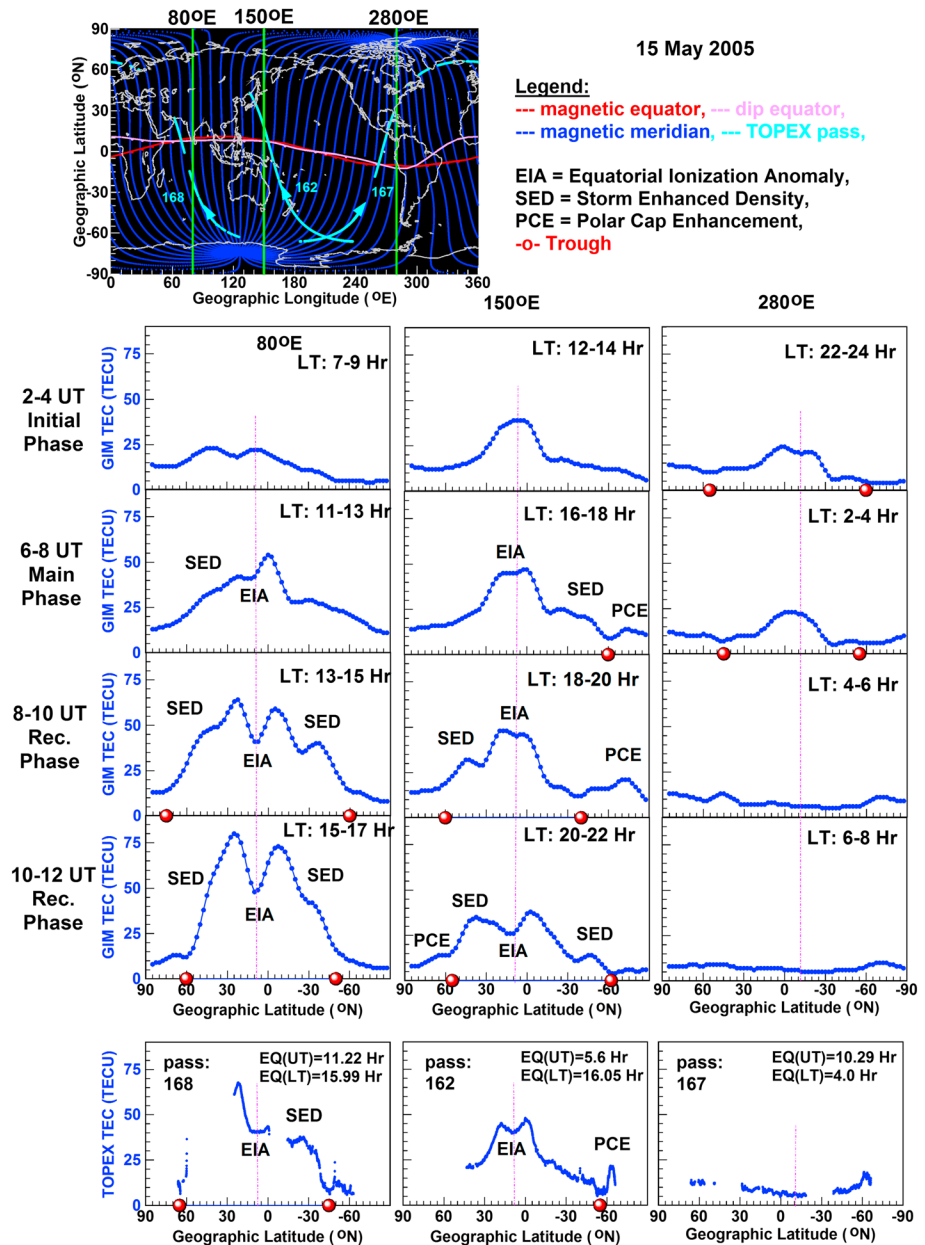
Figure 3. (top) The global map depicts the ground tracks of the TOPEX passes shown and the geographic longitude sectors investigated. (bottom) Some latitudinal GIM TEC profiles constructed for 80°E, 150°E, and 280°E illustrate together with some matching TOPEX TEC line plots how the ionosphere varied as the storm unfolded.

near Alaska and its southern counterpart during 0400–1000 UT. For maps 4 and 5, we have also plotted the auroral oval boundaries.

According to our interpretation, these TEC maps demonstrate that as the storm was unfolding, and as the w-EEJ became intensified in the American sector during the local midnight-dawn hours, the plasma density became more depleted over the Western Hemisphere. Oppositely, plasma densities became significantly enhanced in the daytime Eastern Hemisphere as the e-EEJ became stronger in the Indian-Australian sector.

Figure 3 illustrates a global map where the ground tracks of some TOPEX passes are plotted with the magnetic meridian and magnetic and dip equators. Representing the longitude sectors investigated, the geographic longitudes of 80°E, 150°E, and 280°E are highlighted. Regarding the line plots, a set of TEC latitudinal line
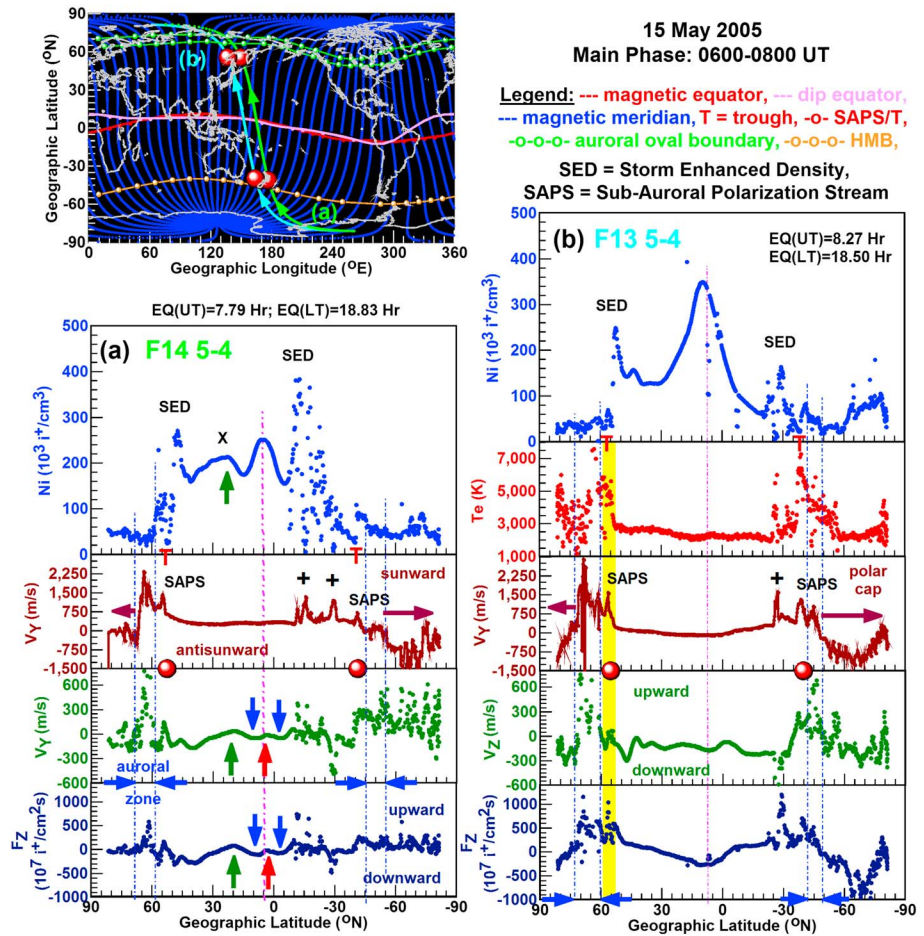
Figure 4. The global map shows the ground tracks of (a) F14 and (b) F13 spacecraft, and the locations of midlatitude trough. A set of multi-instrument line plots depict at ~1800 LT during the main phase the EIA and SED appearing in the topside ionosphere, their underlying plasma flows and drift, and their thermal characteristics. At SED latitudes, the scattered Ni data imply structured SED plume plasma. Underlying midlatitude plasma bubbles are implied by the increased sunward drifts (marked as plus). The enhanced Ni (marked as cross; underlying upward drifts/flows are indicated by green arrows) is the signature of a positive storm phase, occurring equatorward of the SED. The shaded interval in yellow highlights the SAPS-related westward drift and upward drifts and flux. Red and blue arrows mark the forward fountain-related vertical plasma drifts/flows. EQ(UT) and EQ(LT) indicate equator crossing universal time and local time, respectively, in decimal hours.

plots are constructed with GIM TEC and TOPEX TEC values for these longitude sectors. These latitudinal TEC plots tracked the EIA's two-peak structure, the SED appearing equatorward of the midlatitude trough (indicated as red dot), and the polar cap enhancement (PCE) situated poleward of the trough. These line plots depict the best development of EIA (~75 TECU) and SED (~40 TECU) in the Indian sector during the local afternoon and evening hours as the storm progressed from the main phase to the recovery phase. In the Australian sector, the features of SED and PCE became better developed, and the EIA appeared first in a weaker form (~40 TECU) in the recovery phase. Oppositely, the TEC became depleted (~5 TECU) in the American sector during the local dawn-morning hours under w-EEJ conditions in the recovery phase. Meanwhile, the TOPEX TEC line plots show close similarities to their matching—both in time and in space—GIM TEC profiles. These similarities indicate the accuracy of GIM TEC data that are interpolated in space and time in order to produce continuous maps [*Mannucci et al.*, 1998]. We also note here that there is an approximate 2 h time delay between the e-EEJ and EIA variations.

3.3. EIA and SED Development in the Australian Sector During the Local Evening Hours

Figure 4 is constructed for the Australian sector with DMSP F14 (see Figure 4a) and F13 (see Figure 4b) data that cover different UTs but similar LTs (~1830 LT) over the eastern Pacific (see global map). In this way, we could observe some temporal variations under strong e-EEJ conditions as the main phase progressed
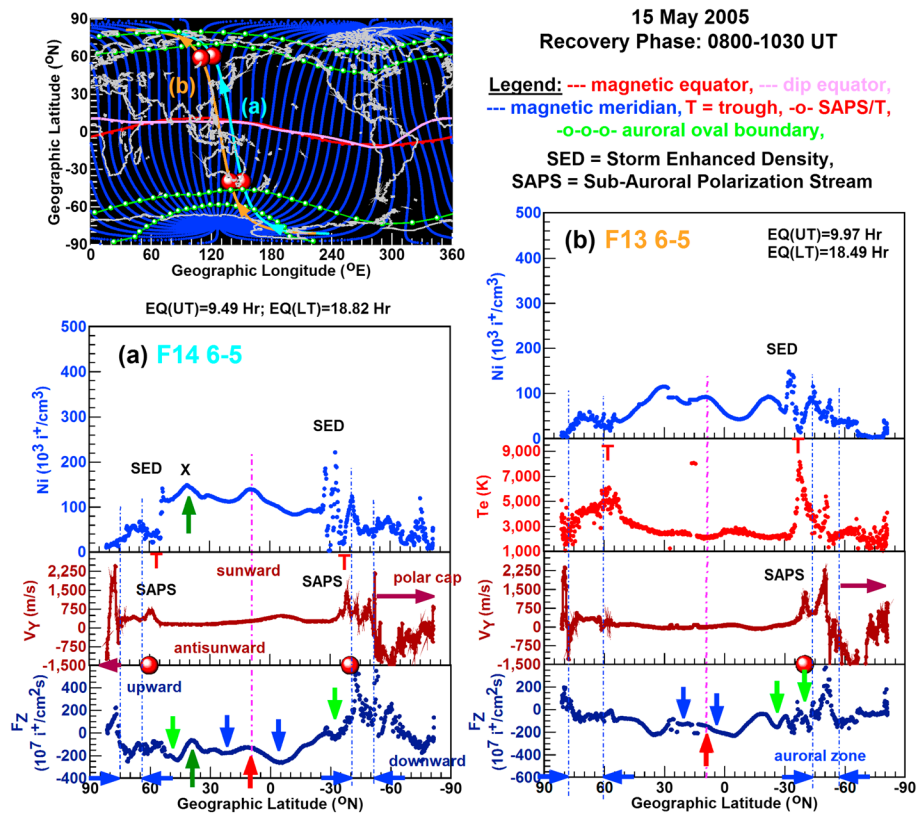
Figure 5. The same as Figure 4 but for the recovery phase. During the recovery phase, the positive storm phase (marked as cross) in the north became better developed than the SED, but the SED plume plasma was still structured as implied by the scattered Ni data as shown in Figure 5a. SED-related downward plasma flows are indicated by the light green arrows.

toward the recovery phase. The global map illustrates the ground tracks of DMSP passes analyzed, the auroral oval boundary positions at 0815 UT in the north, and the Heppner-Maynard boundary (HMB) indicating the equatorward oval boundary [*Heppner and Maynard*, 1987] in the south due to the absence of OVATION data for that UT range.

In each panel, the Ni line plot illustrates that the EIA appeared as a single-peak feature ($\sim 300 \times 10^3$ i$^+$/cm^3) in the topside ionosphere. Close to it, a local Ni enhancement (indicated as "cross"; see Figure 4a) appeared that was possibly created by some upward drifts and plasma flows (indicated as green arrow; see Figure 4a and details below) due to traveling ionospheric disturbances (TIDs). Such enhanced plasma density is also known as positive phase [*Prölss et al.*, 1991] and usually, as in this case, appears equatorward of the SED. A well-formed SED feature developed on the midlatitude trough's equatorward edge. In the south, the SED feature was particularly large ($\sim 400 \times 10^3$ i$^+$/cm^3; see Figure 4a). There, the scattered data indicate midlatitude plasma structuring due to the R-T instability conditions created by the eastward PPEF and causing the development of midlatitude plasma bubbles [*Foster and Rich*, 1998]. Shown by the T_e line plot in Figure 4b, the location of trough is marked by the subauroral T_e peak (~ 7000 K) that is a quasi-permanent feature of the topside ionosphere [*Prölss*, 2006]. By utilizing the V_Y line plot, we have specified (1) the enhanced sunward (or westward) drifts (~ 1500 m/s; indicated as "plus") associated with the midlatitude bubbles [*Foster and Rich*, 1998], (2) the SAPS **E** field signature appearing as a sunward peak where the trough minimum is [*Foster and Burke*, 2002], (3) the auroral convection appearing as a sunward peak in the auroral zone, (4) the auroral zone's equatorward boundary that is situated poleward of the SAPS signature, and (5) the convection reversal boundary where the sunward convection turns to antisunward and thus marks the poleward boundary of the auroral zone or the equatorward boundary of the polar cap region [*Heelis and Mohapatra*, 2009; *Horvath and Lovell*, 2009]. Meanwhile, the V_Z and F_Z line plots (see Figure 4a) tracked the forward fountain's vertical plasma drift and plasma flows underlying the EIA. Based on the modeling work of *Balan and Bailey* [1995], the upward drift/flow (indicated as red arrow) is driven by the equatorial upward
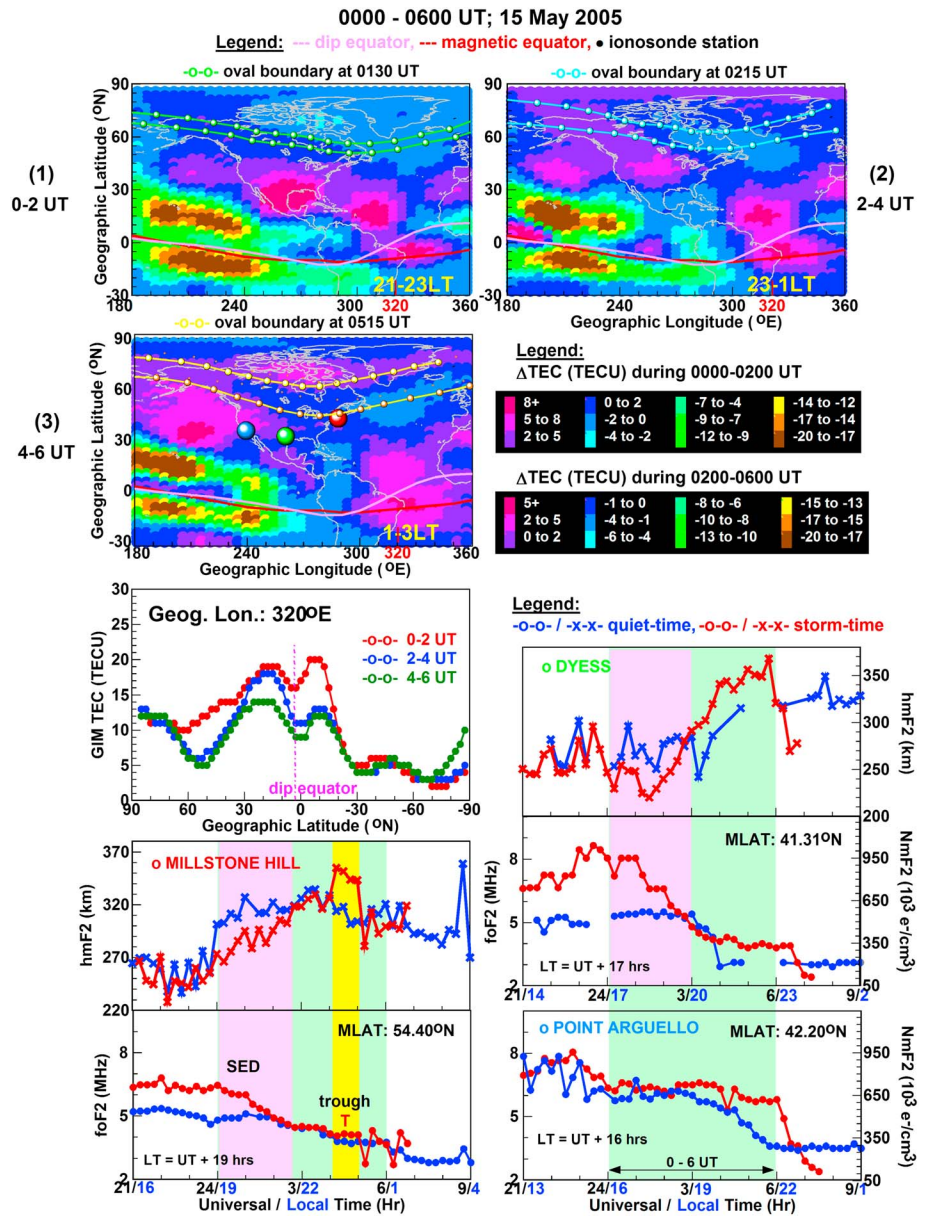
Figure 6. (top) The ΔTEC map series demonstrates in 2 h intervals the spatial variation of EIA, SED plume, and positive storm prior to and during the initial phase. Map 3 illustrates the locations of ionosonde stations providing ionosonde data. (bottom) The GIM TEC line plots show latitudinal variations over the Atlantic and depict the well-developed EIA and some increased TECs in the northern polar cap region. A series of f_oF_2 and N_mF_2 line plots show F_2 region plasma density variations in UT over a few northern stations. The time interval covered by the ΔTEC maps is indicated by the shaded interval in green. For Dyess and Millstone Hill, the f_oF_2 and h_mF_2 measurements demonstrate the expansion of the polar convection, during which the SED (indicated as shaded interval in pink) and the midlatitude trough (indicated ad shaded interval in yellow) passed over the station.

$E \times B$ drift, and the downward drift/flow at each EIA crest location (indicated as blue arrow) is due to the field-aligned plasma drift/flow driven by gravity and pressure gradient forces. As downward drifts/flows are quite close to the dip equator, the EIA appeared as a single-peak structure. Furthermore, these fountain-related plasma drifts/flows are not obvious in Figure 4b at all because of the strong modulating effects of TIDs. Both panels' V_Z line plots tracked some prominent TIDs propagating equatorward and poleward from the auroral zone ($T_e \approx 5000$ K) where they were possibly generated by intense Joule heating [*Hunsucker*, 1982].

Figure 5 is constructed for the Australian sector in a similar fashion with F14 and F13 passes for an early stage of the recovery phase, at ~1830 LT but at different UTs, when the e-EEJ was weaker. In the global map, the
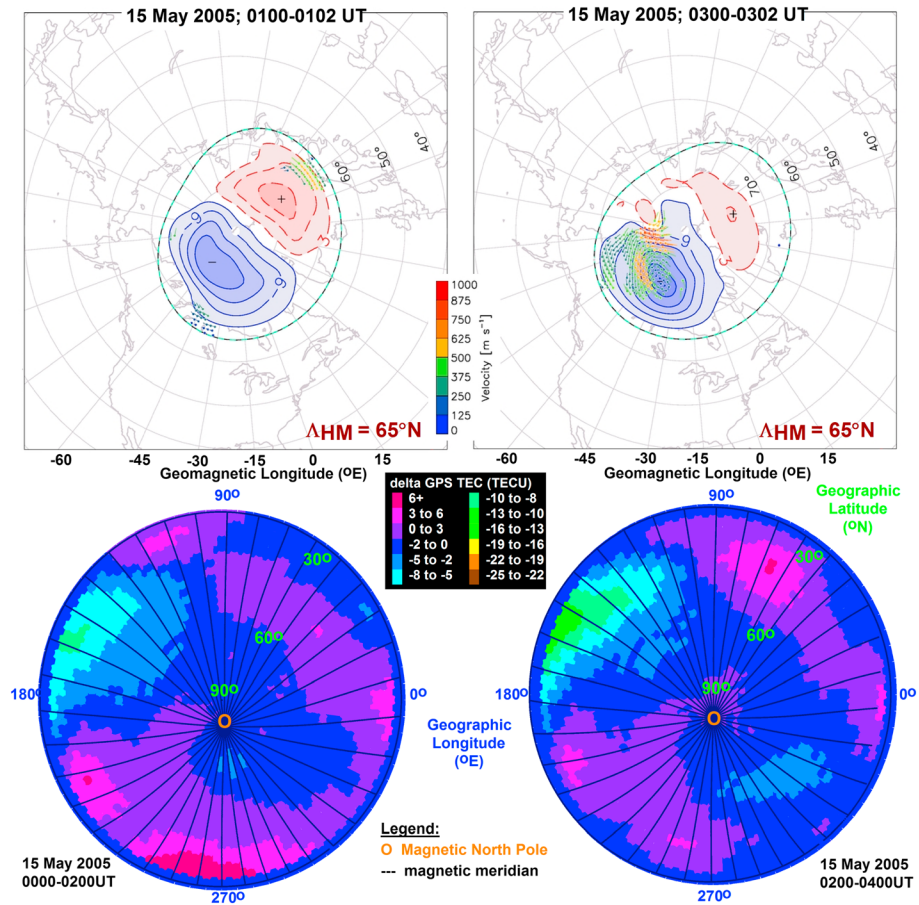
Figure 7. (top) Two scenarios illustrate, with large-scale convection maps constructed for the Northern Hemisphere, that a two-cell convection pattern had been operational prior to and during the initial phase over the northern polar cap. In each map, the location of Heppner-Maynard boundary (Λ_{HM}; invariant latitudes) is indicated. (bottom) During each scenario, the polar ΔTEC plot tracked a well-formed polar TOI reaching the magnetic North Pole. The polar plots show also the magnetic meridians and the location of magnetic North Pole.

oval boundaries are plotted for 0940 UT in the north and for 1150 UT in the south. Both the single-peak structure of the EIA ($\sim 150 \times 10^3$ i$^+$/cm^3) and the SED features ($\sim 200 \times 10^3$ i$^+$/cm^3) became less developed than earlier in the main phase (see Figure 4), but the TID-related midlatitude Ni enhancement (i.e., positive phase; indicated as cross) became better developed than the SED. Furthermore, the SED plume plasma was still structured in the south because of some midlatitude plasma bubbles. But this time, the bubble-related increased sunward drift, and the SAPS **E** field signature appeared together as a single sunward peak ($V_Y \approx 1500$ m/s).

3.4. SED and TOI Development in the American Sector During the Local Evening Hours

We have further investigated SED and TOI development by constructing 2-hourly GIM ΔTEC maps with TEC$_{(storm\ time)}$ − TEC$_{(quiet\ time)}$ values. Figure 6 shows a series of three 2-hourly ΔTEC maps covering a larger region of the North American continent during the disturbed ($Kp = 6$) prestorm period of 0000–0600 UT plus the auroral oval boundaries at 0130, 0215, and 0515 UT, respectively. With the largest ΔTEC values (indicated in red and pink), these maps tracked the EIA crests over the Atlantic illustrating a well-developed EIA there plus some plasma density enhancements that appeared first over the Caribbean (see map 1) and drifted later on westward and sunward (see maps 2 and 3). These ΔTEC maps tracked also some smaller plasma density increases close to Alaska (2–5 and 0–2 TECU; indicated in purple and blue, respectively; see map 1) that later on drifted into the polar region (2–5 and 0–2 TECU; indicated in pink and purple, respectively, see maps 2 and 3) and contributed to the formation of a polar TOI (see details in section 3.5).

In order to further illustrate the well-developed EIA appearing over the Atlantic, three GIM TEC latitudinal profiles are constructed for 320°E by utilizing data from maps 1–3 shown in Figure 2. Meanwhile, ΔTEC
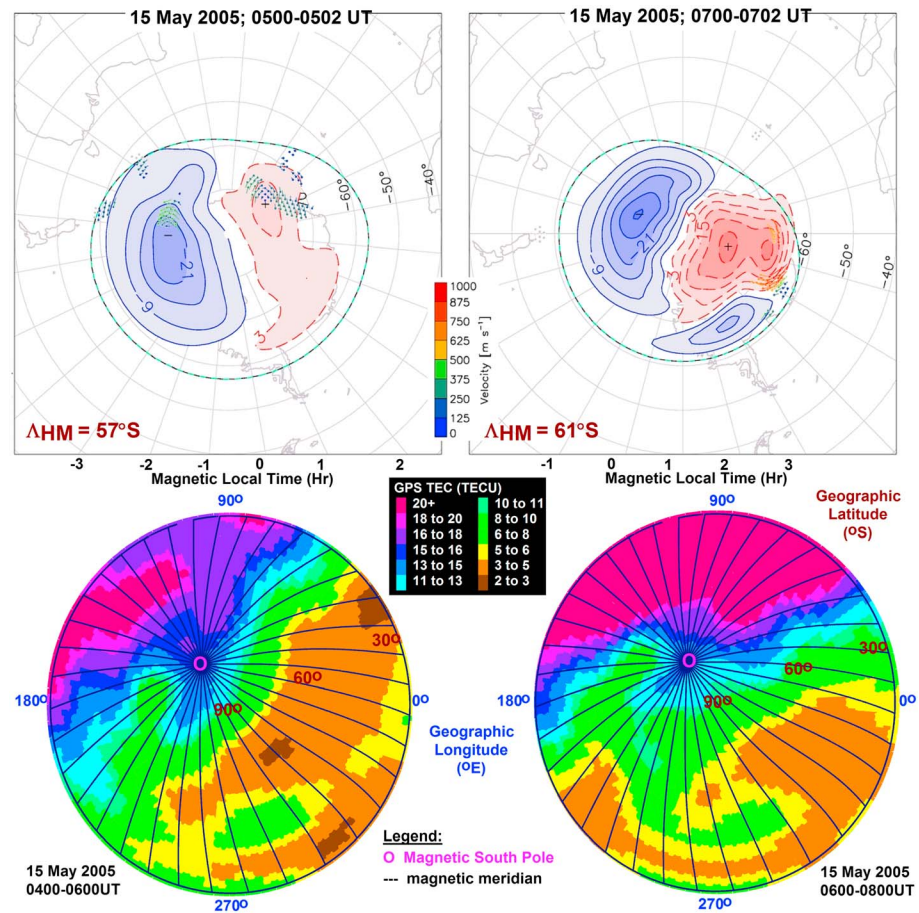
Figure 8. Same as Figure 7 but for the Southern Hemisphere during the initial phase and the main phase with GIM TEC data. An important feature is that during these scenarios, the polar TOI progressed over the magnetic pole and into the nightside and remained well developed in the antisunward flow channel.

map 3 depicts three ionosonde stations situated in the path of this westward moving enhanced TEC region. A series of f_oF_2 line plots, where the N_mF_2 values are also indicated, demonstrates that the storm time plasma density (indicated in red) increased with respect to the quiet time values (indicated in blue). Some earlier increases were detected at Millstone Hill (~23%; 0000–0230 UT) and Dyes (~45%; 0000–0130 UT) while some later increases were seen at Point Arguello (~15%; 0300–0700 UT) as the enhanced plasma density propagated over these stations from east to west. Since the Millstone Hill station was close to the equatorward auroral oval boundary, it possibly measured SED effects earlier and SAPS effects later as the auroral oval expanded (see mapped oval positions in the ΔTEC maps). Thus, an earlier SED detection (0000–0245 UT; indicated as shaded interval in pink) was followed by the later detection of midlatitude trough (0400–0500 UT; indicated as shaded area in yellow) located in the SAPS channel (see details in section 3.3). This interpretation is further demonstrated with the h_mF_2 line plots accompanying the N_mF_2 plots where the quiet time levels are also shown. The earlier SED effects (0000–0245 UT) are indicated by the simultaneous increase of N_mF_2 and decrease of h_mF_2, as the downward flowing SED plume plasma decreased the F_2 layer height and increased the F_2 layer plasma density. The later SAPS effects (0400–0500 UT) are illustrated with minimum N_mF_2 and increased h_mF_2, as the upward drift in the SAPS channel suddenly increased the F_2 layer height while the F_2 layer plasma density became depleted in the trough region.

3.5. Mapping Polar TOI and Polar Convection During 0000–0400 and 0400–0800 UT

In order to further investigate the pattern of plasma density distribution in the context of two-cell plasma convection, we have employed the Super Dual Auroral Radar Network (SuperDARN) polar potential mapping technique and generated some polar convection maps via interactive plotting. For the Northern

Hemisphere, the plotting times of 0100 and 0300 UT gave median convection scenarios suitable for two of the above-described regional GIM ΔTEC maps tracking SED and TOI features during 0000–0200 and 0200–0400 UT, respectively (see details in section 3.4). In Figure 7, the convection maps are shown with the GIM ΔTEC polar plots where the magnetic meridians are also graphed. In both prestorm scenarios, the negative convection cell developed over the northern region of North America and the dayside cusp was situated close to Alaska (1330–1730 LT). As a small increase, the SED plume plasma (0–3 TECU; indicated in purple) appeared and was transported by antisunward convection from the nightside through the dayside cusp into the polar region and to the magnetic North Pole. Figure 8 is constructed in a similar fashion for the Southern Hemisphere and shows an initial phase scenario (0400–0600 UT) and a main phase scenario (0600–0800 UT) for which the SuperDARN plotting times are 0500 and 0700 UT, respectively. For a better presentation, we have utilized GIM TEC values for polar map plotting. These maps illustrate that the negative cell developed in the Australian longitude sector and that some SED plume plasma (13–15 TECU; indicated in blue) entered the polar region via the dayside cusp (at ~120°E, near Casey; 1200–1600 LT) and became transported by the antisunward convection deep inside the polar cap where it formed a narrow polar TOI progressing over the magnetic South Pole into the nightside.

4. Discussions

Observational results presented in this study reveal that the 15 May 2005 geomagnetic superstorm was quite special because of its disturbed prestorm period (0000–0300 UT) and long-duration initial phase (0300–0600 UT), during which a polar cap substorm [*Kozyreva and Kleimenova*, 2007] occurred. As our results demonstrate and therefore add to the findings of *Kozyreva and Kleimenova* [2007], the IEF E_Y component carried these hydromagnetic waves, and its effects penetrated to the auroral region and from there both to the polar region and to the equator. There, its equatorial signatures appeared as a w-EEJ in the daytime Indian-Australian sector and as an e-EEJ in the nighttime American sector. Our results reveal also the development of some ionospheric features during this 0000–0600 UT period, before the main phase, such as SED and polar TOI that are expected to occur during a main phase and under the effects of a strong PPEF.

First, we discuss the SED and polar TOI features (see ΔTEC maps in Figure 6) occurring prior to the main phase, during 0000–0600 UT, in the American sector where the conditions are naturally favorable due to the magnetic field geometry [*Foster*, 1993; *Sojka et al.*, 2012]. Under increasing magnetic activity, as the substorm unfolded during 0000–0600 UT, the convection pattern continuously expanded due to the increasing convection **E** field as implied by the modeled Φ_{PC} showing increases (from 30 to 80 kV prior to and from 80 to 230 kV during the initial phase). Consequently, the polar cap boundary moved equatorward, to 65°N (geomagnetic), and thus extended into the sunlit region. Furthermore, the evening EIA had become well developed over the Atlantic (see ΔTEC map 1 in Figure 6) because of the unusually strong equatorial upward **E** × **B** drift ($V_Z \approx |\mathbf{E} \times \mathbf{B}|/B^2$) created in the SAMA region [*Foster and Erickson*, 2013] by the interaction of weak magnetic **B** field and combined strong evening (~2100 LT) eastward polarization and disturbance **E** fields. At ~2100 LT (0100 UT), these well-developed EIA crests supplied high-density ionospheric plasma that traveled quite a long way by drifting westward from the Atlantic, across the North American continent, to the dayside cusp that was situated at that time close to Alaska. This westward drifting plasma provided a significant contribution to the development of SED and polar TOI. But some enhanced TECs developed in the daytime sector, close to the dayside cusp (near Alaska; see ΔTEC map 3 in Figure 6), and contributed also to the development of polar plasma density enhancements by supplying fresh solar-produced ionospheric source plasma to the dayside cusp inflow region. Although the polar TOI reached the magnetic North Pole, it did not propagate deeper into the polar cap region along the antisunward flow channel (see Figure 7). Oppositely on the dayside of the Southern Hemisphere and still during the initial phase, the polar TOI appeared to be better developed as it propagated over the magnetic South Pole and into the nightside of the polar cap region (see Figure 8, left). To explain these strong hemispherical differences seen in SED and TOI development prior to and during the initial phase, we highlight three geophysical factors that created locally more favorable conditions in the south: (1) the convection boundary moved to lower latitudes (~60°S) compared to the northern boundary (at 65°N), (2) the high-density SED plume plasma developed close to the dayside cusp and thus (3) traveled less before entering the polar cap region.

Another important result to discuss is the detection of a large northern SED plume over Asia during the local afternoon hours of the main phase (see GIM TEC map 4 in Figure 2) that became better developed during the local evening hours of the recovery phase (see GIM TEC map 5 in Figure 2) but did not lead to any polar TOI development in the north. Adding to previous studies investigating the development of SED plume outside the American longitude sector (see details in section 1), our results demonstrate that the increasingly better development of SED plume over Asia was due to some local electrodynamic factors (e.g., strong equatorial $\mathbf{E} \times \mathbf{B}$ uplift, strong SAPS $\mathbf{E}$ field effects, and expansion of polar convection), while the geomagnetic storm unfolded. To discuss these electrodynamic factors, the $\mathbf{E} \times \mathbf{B}$ uplift of the ionosphere in the Asian sector was strong due to the strong eastward net $\mathbf{E}$ field ($\delta\Delta H \approx 120$ nT; see Figure 1) over India. During the local evening hours, this strong net $\mathbf{E}$ field was possibly due to the combined effects of eastward PPEF and evening eastward polarization $\mathbf{E}$ field. Furthermore, the SAPS $\mathbf{E}$ field was also strong ($V_Y \approx 1500$ m/s), as was observed in the Australian sector (see Figure 4), and was able to drive the SED plume plasma sunward and toward the dayside cusp. Moreover, the polar convection boundary extended to 50°N and remained in the 50–55°N range for a few hours implying both the strong erosion of the plasmasphere and the sunlit location of the polar cap boundary in the dusk cell. Although the storm time EIA-SED structure became better formed over both hemispheres in the Asian longitude sector by the beginning of the recovery phase, the polar TOI developed only in the south.

Finally we discuss the absence of polar TOI in the north and its presence in the south during this main phase/recovery phase interface period. Starting with the northern scenario, we try to find out why the above-described well-formed EIA-SED plume structure in the north did not lead to a polar TOI development. We consider (1) the position of the negative dusk cell that was situated over Asia and (2) the location of the dayside cusp inflow region that moved from Scandinavia toward Greenland. Thus, the SED plume plasma was the farthest away from the magnetic North Pole and therefore could not reach the dayside cusp inflow region. Consequently, this geometry did not support the development of polar TOI in the north. The main reason is that as the SED plume plasma traveled this longest distance, it had been in the dark for an extended period of time, causing the rapid decrease of its plasma density due to fast recombination. These observational results add to the recent modeling study of *Sojka et al.* [2012] that demonstrates the crucial roles of solar zenith angle and distance traveled in determining the degree of development of plasma density enhancements. Continuing with the Southern Hemisphere observations, an opposite scenario occurred in the south, since the Asian-Australian longitude sector is situated closest to the magnetic South Pole. During the main phase/recovery phase interphase, the polar convection boundary developed at ~50°S. As the SED plume plasma (18–22 TECU; indicated in green in maps 4–5 in Figure 2) traveled less to reach the dayside cusp, the SED plume was still well developed when it entered the polar cap region and formed a polar TOI that progressed over the magnetic South Pole from the dayside deep into the nightside polar cap region (see Figure 8, right).

5. Conclusions

We have investigated comprehensively the global response of the ionosphere to the 15 May 2005 superstorm by studying the underlying electrodynamics and the resultant plasma distribution. Our observational results demonstrate that this geomagnetic superstorm was quite unique, and its unique storm features produced some interesting ionospheric responses.

1. Its early substorm ($Kp = 6-$; $B_Z = -5$ nT) and following polar cap substorm ($Kp = 6-$) produced in both hemispheres the ionospheric features of SED plume and polar TOI, which are expected to develop during the main phase under the influence of a strong PPEF.
2. During its early substorm period (0000–0600 UT; $Kp = 6-$), the solar wind-generated hydromagnetic waves were carried by the IEF $\mathbf{E_Y}$ component. The effects of IEF penetrated to the auroral region and from there to the polar cap and also to the equator producing some well-defined w-EEJ at daytime in the Indian-Australian sector and e-EEJ at nighttime in the American sector. Adding to previous studies, we report first these EEJ signatures of the hydromagnetic wave effects.
3. Its main phase (0600–0800 UT; $Kp = 8+$) produced a well-developed EIA-SED plume structure outside the American sector, in the Asian-Australian longitude sector, and over both hemispheres.

4. During its early recovery phase ($Kp = 8-$), this EIA-SED plume structure became better developed over both hemispheres, but the polar TOI developed only in the south where the SED plume was close to both the dayside cusp providing an entry into the polar cap region and the magnetic South Pole. Oppositely in the north, the polar TOI was absent due to the longest distance between the dayside cusp and the magnetic pole.

Finally, we conclude that this unique storm with its unique storm features allowed us to gain new insights into various physical processes underlying the development of SED and polar TOI. These new insights add to previous studies, fill knowledge gaps, and suggest further research directions such as more detailed investigations covering ionospheric electrodynamics and plasma distribution in the context of storm time electrodynamics. Our results are valuable because (1) there are only a few studies investigating SED and TOI developments outside the American sector, and most of those studies focus on repeatability and similarities and not differences; (2) we have provided evidence that the different hemispherical and longitudinal characteristics of the SED plume and polar TOI structure were created by the local electrodynamic and geophysical conditions that were quite different; and (3) this is the first report providing observational evidence that the SED plume TOI structure occurred with different characteristics during each storm phase (i.e., initial phase, main phase, and early recovery phase).

References

Ahn, B.-H., S.-I. Akasofu, and Y. Kamide (1983), The Joule heat production rate and the particle energy injection rate as a function of the geomagnetic indices AE and AL, *J. Geophys. Res.*, *88*(A8), 6275–6287, doi:10.1029/JA088iA08p06275.

Anderson, D., K. Yumoto, M. Ishitsuka, and E. Kudeki (2002), Estimating daytime vertical E × B drift velocities in the equatorial *F*-region using ground-based magnetometer observations, *Geophys. Res. Lett.*, *29*(12), 1596, doi:10.1029/2001GL014562.

Balan, N., and G. J. Bailey (1995), Equatorial plasma fountain and its effects: Possibility of an additional layer, *J. Geophys. Res.*, *100*(A11), 21,421–21,432, doi:10.1029/95JA01555.

Balan, N., K. Shiokawa, Y. Otsuka, T. Kikuchi, D. Vijaya Lekshmi, S. Kawamura, M. Yamamoto, and G. J. Bailey (2010), A physical mechanism of positive ionospheric storms at low and mid latitudes, *J. Geophys. Res.*, *115*, A02304, doi:10.1029/2009JA014515.

Balan, N., Y. Otsuka, M. Nishioka, J. Y. Liu, and G. J. Bailey (2013), Physical mechanisms of the ionospheric storms at equatorial and higher latitudes during the recovery phase of geomagnetic storms, *J. Geophys. Res. Space Physics*, *118*, 2660–2669, doi:10.1002/jgra.50275.

Basu, S., et al. (2001), Ionospheric effects of major magnetic storms during the international space weather period of September and October 1999: GPS observations, VHF/UHF scintillations and in situ density structures at middle and equatorial latitudes, *J. Geophys. Res.*, *106*(A12), 30,389–30,413, doi:10.1029/2001JA001116.

Basu, S., et al. (2005), Two components of ionospheric plasma structuring at midlatitudes observed during the large magnetic storm of October 30, 2003, *Geophys. Res. Lett.*, *32*, L12S06, doi:10.1029/2004GL021669.

Basu, S., S. Basu, F. J. Rich, K. M. Groves, E. MacKenzie, C. Coker, Y. Sahai, P. R. Fagundes, and F. Becker-Guedes (2007), Response of the equatorial ionosphere at dusk to penetration electric fields during intense magnetic storms, *J. Geophys. Res.*, *112*, A08308, doi:10.1029/2006JA012192.

Basu, S., S. Basu, E. MacKenzie, C. Bridgwood, C. E. Valladares, K. M. Groves, and C. Carrano (2010), Specification of the occurrence of equatorial ionospheric scintillations during the main phase of large magnetic storms within solar cycle 23, *Radio Sci.*, *45*, RS5009, doi:10.1029/2009RS004343.

Bisi, M. M., et al. (2010), From the Sun to the Earth: The 13 May 2005 coronal mass ejection, *Sol. Phys. A J. Sol. Sol.-Stellar Res. Study Sol. Terr. Phys.*, *265*(1), 49–127, doi:10.1007/s11207-010-9602-8.

Blanc, M., and A. Richmond (1980), The ionospheric disturbance dynamo, *J. Geophys. Res.*, *85*(A4), 1669–1686, doi:10.1029/JA085iA04p01669.

Coster, A. J., M. J. Colerico, J. C. Foster, W. Rideout, and F. Rich (2007), Longitude sector comparisons of storm enhanced density, *Geophys. Res. Lett.*, *34*, L18105, doi:10.1029/2007GL030682.

Dashora, N., S. Sharma, R. S. Dabas, S. Alex, and R. Pandey (2009), Large enhancements in low latitude total electron content during 15 May 2005 geomagnetic storm in Indian zone, *Ann. Geophys.*, *27*, 1803–1820, doi:10.5194/angeo-27-1803-2009.

Davies, K., and X. M. Liu (1991), Ionospheric slab thickness in middle and low latitudes, *Radio Sci.*, *26*(4), 997–1005, doi:10.1029/91RS00831.

Foster, J. C. (1993), Storm time plasma transport at middle and high latitudes, *J. Geophys. Res.*, *98*(A2), 1675–1689, doi:10.1029/92JA02032.

Foster, J. C. (2008), Ionospheric-magnetospheric-heliospheric coupling: Storm-time thermal plasma redistribution, in *Mid-Latitude Dynamics and Disturbances, Geophys. Monogr. Ser.*, vol. 181, edited by P. M. Kintner et al., pp. 121–134, AGU, Washington, D. C., doi:10.1029/181GM12.

Foster, J. C., and W. J. Burke (2002), SAPS: A new characterization for sub-auroral electric fields, *Eos Trans. AGU*, *83*, 393, doi:10.1029/2002EO000289.

Foster, J. C., and A. J. Coster (2007), Conjugate localized enhancement of total electron content at low latitudes in the American sector, *J. Atmos. Sol. Terr. Phys.*, doi:10.1016/j.jastp.2006.09.012.

Foster, J. C., and P. J. Erickson (2013), Ionospheric superstorms: Polarization terminator effects in the Atlantic sector, *J. Atmos. Sol. Terr. Phys.*, *103*, 147–156, doi:10.1016/j.jastp.2013.04.001.

Foster, J. C., and F. J. Rich (1998), Prompt midlatitude electric field effects during severe geomagnetic storms, *J. Geophys. Res.*, *103*(A11), 26,367–26,372, doi:10.1029/97JA03057.

Foster, J. C., and H. B. Vo (2002), Average characteristics and activity dependence of the subauroral polarization stream, *J. Geophys. Res.*, *107*(A12), 1475, doi:10.1029/2002JA009409.

Foster, J. C., P. J. Erickson, A. J. Coster, J. Goldstein, and F. J. Rich (2002), Ionospheric signatures of plasmaspheric tails, *Geophys. Res. Lett.*, *29*(13), 1623, doi:10.1029/2002GL015067.

Foster, J. C., et al. (2005), Multiradar observations of the polar tongue of ionization, *J. Geophys. Res.*, *110*, A09S31, doi:10.1029/2004JA010928.

Gonzalez, W. D., B. T. Tsurutani, and A. L. C. Conzalez (1999), Interplanetary origin of geomagnetic storms, *Space Sci. Rev.*, *88*, 529–562, doi:10.1023/A:1005160129098.

Heelis, R. A., and S. Mohapatra (2009), Storm time signatures of the ionospheric zonal ion drift at middle latitudes, *J. Geophys. Res.*, *114*, A02305, doi:10.1029/2008JA013620.

Heppner, J. P., and N. C. Maynard (1987), Empirical high-latitude electric field models, *J. Geophys. Res.*, *92*(A5), 4467–4489, doi:10.1029/JA092iA05p04467.

Horvath, I. (2006), A total electron content space weather study of the nighttime Weddell Sea Anomaly of 1996/1997 southern summer with TOPEX/Poseidon radar altimetry, *J. Geophys. Res.*, *111*, A12317, doi:10.1029/2006JA011679.

Horvath, I. (2007), Impact of 10 January 1997 geomagnetic storm on the nighttime Weddell Sea Anomaly: A study utilizing data provided by the TOPEX/Poseidon mission and the Defense Meteorological Satellite Program, and simulations generated by the Coupled Thermosphere/Ionosphere Plasmasphere model, *J. Geophys. Res.*, *112*, AO6329, doi:10.1029/2006JA012153.

Horvath, I., and B. C. Lovell (2009), Distinctive plasma density features of the topside ionosphere and their electrodynamics investigated during southern winter, *J. Geophys. Res.*, *114*, A01304, doi:10.1029/2008JA013683.

Huang, C.-S., O. de La Beaujardiere, P. A. Roddy, D. E. Hunton, J. O. Ballenthin, and M. R. Hairston (2012), Generation and characteristics of equatorial plasma bubbles detected by the C/NOFS satellite near the sunset terminator, *J. Geophys. Res.*, *117*, A11313, doi:10.1029/2012JA018163.

Hunsucker, R. D. (1982), Atmospheric gravity waves generated in the high-latitude ionosphere: A review, *Rev. Geophys.*, *20*(2), 293–315, doi:10.1029/RG020i002p00293.

Kelley, M. C., B. G. Fejer, and C. A. Gonzales (1979), An explanation for anomalous ionospheric electric fields associated with a northward turning of the interplanetary magnetic field, *Geophys. Res. Lett.*, *6*(4), 301–304, doi:10.1029/GL006i004p00301.

Kozyreva, O. V., and N. G. Kleimenova (2007), Geomagnetic pulsations and magnetic disturbances during the initial phase of a strong magnetic storm of May 15, 2005 Disturbances during the Initial Phase of a Strong Magnetic Storm of May 15, 2005.

Mannucci, A. J., B. D. Wilson, D. N. Yuan, C. H. Ho, U. J. Lindqwister, and T. F. Runge (1998), A global mapping technique for GPS-derived ionospheric electron content measurements, *Radio Sci.*, *33*(3), 565–582, doi:10.1029/97RS02707.

Mannucci, A. J., B. T. Tsurutani, B. A. Iijima, A. Komjathy, A. Saito, W. D. Gonzalez, F. L. Guarnieri, J. U. Kozyra, and A. Skoug (2005), Dayside global ionospheric response to the major interplanetary events of October 29–30, 2003 "Halloween Storms", *Geophys. Res. Lett.*, *32*, L12S02, doi:10.1029/2004GL021467.

Maruyama, T. (2006), Extreme enhancement in total electron content after sunset on 8 November 2004 and its connection with storm enhanced density, *Geophys. Res. Lett.*, *33*, L20111, doi:10.1029/2006GL027367.

Moen, J., X. C. Qiu, H. C. Carlson, R. Fujii, and I. W. McCrea (2008), On the diurnal variability in F2-region plasma density above the EISCAT Svalbard radar, *Ann. Geophys.*, *26*, 2427–2433, doi:10.5194/angeo-26-2427-2008.

Orus, R., M. Hernandez-Pajares, J. M. Juan, and J. Sanz (2005), Improvement of global ionospheric VTEC maps by using kriging interpolation technique, *J. Atmos. Sol. Terr. Phys.*, *67*(16), 1598–1609, doi:10.1016/j.jastp.2005.07.017.

Ott, E. (1978), Theory of Rayleigh-Taylor bubbles in the equatorial ionosphere, *J. Geophys. Res.*, *83*(A5), 2066–2070, doi:10.1029/JA083iA05p02066.

Palmroth, M., T. I. Pulkkinen, P. Janhunen, D. J. McComas, C. W. Smith, and H. E. J. Koskinen (2004), Role of solar wind dynamic pressure in driving ionospheric Joule heating, *J. Geophys. Res.*, *109*, A11302, doi:10.1029/2004JA010529.

Prölss, G. W. (2006), Subauroral electron temperature enhancement in the nighttime ionosphere, *Ann. Geophys.*, *24*(7), 1871–1885, doi:10.5194/angeo-24-1871-2006.

Prölss, G. W., L. H. Brace, H. G. Mayr, G. R. Carignan, T. L. Killeen, and J. A. Klobuchar (1991), Ionospheric storm effects at subauroral latitudes: A case study, *J. Geophys. Res.*, *96*(A2), 1275–1288, doi:10.1029/90JA02326.

Russell, C. T., and M. Ginskey (1995), Sudden impulses at subauroral latitudes: Response for northward interplanetary magnetic field, *J. Geophys. Res.*, *100*(A12), 23,695–23,702, doi:10.1029/95JA02495.

Sojka, J. J., M. David, R. W. Schunk, and R. A. Heelis (2012), A modeling study of the longitudinal dependence of storm time midlatitude dayside total electron content enhancements, *J. Geophys. Res.*, *117*, A02315, doi:10.1029/2011JA017000.

Troshichev, O., H. Hayakawa, A. Matsuoka, T. Mukai, and K. Tsuruda (1996), Cross polar cap diameter and voltage as a function of PC index and interplanetary quantities, *J. Geophys. Res.*, *101*(A6), 13,429–13,435, doi:10.1029/95JA03672.

Tsurutani, B., et al. (2004), Global dayside ionospheric uplift and enhancement associated with interplanetary electric fields, *J. Geophys. Res.*, *109*, A08302, doi:10.1029/2003JA010342.

Vasyliunas, V. M. (1972), The interrelationship of magnetospheric processes, in *Earth's Magnetospheric Processes*, edited by B. M. McCormac, pp. 29–38, D. Reidel, Norwell, Mass.

Yizengaw, E., M. B. Moldwin, and D. A. Galvan (2006), Ionospheric signatures of a plasmaspheric plume over Europe, *Geophys. Res. Lett.*, *33*, L17103, doi:10.1029/2006GL026597.

Yizengaw, E., J. Dewar, J. MacNeil, M. B. Moldwin, D. Galvan, J. Sanny, D. Berube, and B. Sandel (2008), The occurrence of ionospheric signatures of plasmaspheric plumes over different longitudinal sectors, *J. Geophys. Res.*, *113*, A08318, doi:10.1029/2007JA012925.